Alzheimer's Aβ Peptides Containing an Isostructural Backbone Mutation Afford Distinct Aggregate Morphologies but Analogous Cytotoxicity. Evidence for a Common Low-Abundance Toxic Structure(s)?†

Jan Bieschke,‡ Sarah J. Siegel, Yanwen Fu, and Jeffery W. Kelly*

Department of Chemistry and The Skaggs Institute for Chemical Biology, The Scripps Research Institute, 10550 North Torrey Pines Road, La Jolla, California 92037

Received August 29, 2007; Revised Manuscript Received November 5, 2007

ABSTRACT: Amyloid β (Aβ) peptide amyloidogenesis, involving the formation of numerous distinct quaternary structures, appears to cause Alzheimer's disease. However, the precise identification of the toxic structure(s) and the neurotoxicity mechanism(s) remains elusive. Mutating the Aβ 1−40 Phe19−Phe20 backbone amide bond to an isostructural *E*-olefin bond enables formation of spherical aggregates to the exclusion of detectable amyloid fibrils. Herein, the fibrillization and toxicity of amide-to-ester mutants of Aβ 1−40 at the 19−20 position and surrounding backbone amide bonds are compared to the fibrillization and toxicity of the 19−20 *E*-olefin Aβ analogue and wild type Aβ. Whereas isostructural amide-to-*E*-olefin mutations eliminate both the H-bond donor and acceptor capabilities, isostructural amide-to-ester mutations eliminate the donor while retaining the ester carbonyl as a weakened acceptor. None of the amide-to-ester Aβ 1−40 mutants prevent fibrillization; in fact several exhibit hastened amyloidogenesis. The 18−19 amide-to-ester substitution is the only backbone mutation within the hydrophobic core region of the fibril (residues 17−21) that significantly slows fibrillization. Despite forming different morphologies, the 19−20 *E*-olefin mutant, the 18−19 amide-to-ester mutant, and WT Aβ 1−40 fibrils all exhibit similar toxicities when applied to PC12 cells at 18 h into the aggregation reactions, as assessed by MTT metabolic activity measurements. This result suggests that a common but low abundance aggregate morphology, that is accessible to these Aβ analogues, mediates toxicity, or that several different aggregate morphologies are similarly toxic.

Aggregation of the amyloid β (Aβ)[1] peptide into a mixture of quaternary structures, including cross β-sheet amyloid fibrils, is implicated as the cause of Alzheimer's disease based on substantial genetic, biochemical, and pathological evidence (*1*). However, the exact molecular structure of the toxic entity or entities and their mechanism or mechanisms of neurotoxicity remain elusive.

The Aβ family of peptides varying in length and aggregation propensity are produced in the cellular secretory pathway by endoproteolysis of the amyloid precursor protein, a type 1 transmembrane protein (*2*). Extracellular and possibly intracellular Aβ aggregation in the brain, apparently exacerbated by changes brought about by aging, is thought to cause neurodegeneration, possibly through Aβ aggregate-mediated compromises in membrane structure and function (*3*, *4*). While Aβ aggregates into oligomers and higher molecular weight structures including spheres, pores, protofibrils, and amyloid fibrils (*3*), a high-resolution structural model that is supported by numerous lines of experimental evidence, including solid-state NMR and mutagenesis data, is only available for Aβ fibrils (*5*−*7*).

The Aβ fibril structure is stabilized by numerous intra- and intermolecular hydrophobic interactions, intra- and intermolecular salt bridges and numerous intermolecular hydrogen bonds (Figure 1A) (*5*, *6*). Intermolecular backbone−backbone hydrogen bonding is widely observed in both functional and pathologic amyloid fibrils composed of peptides and proteins (*8*−*10*). Hydrogen bonds enveloped by a hydrophobic core and excluded from solvent appear to contribute substantially more to the stability of monomeric folded proteins than do solvent exposed H-bonds (*11*), which is also likely the case for H-bonds in the hydrophobic core of Aβ amyloid fibrils.

The Aβ sequence comprising the hydrophobic core of the cross β-sheet fibril, LVFFA, spanning residues 17−21 (Figure 1A), is believed to be crucial in initiating amyloid

† Research was supported by NIH NS 50636 and DK 46335, the Lita Annenberg Hazen Foundation, the Skaggs Institute of Chemical Biology, and the Bundy Foundation. J.B. was supported by the Max-Planck Society and the Bundy Foundation. S.J.S. was supported by a Norton B. Gilula Fellowship.

* To whom correspondence should be addressed. E-mail: jkelly@scripps.edu. Phone: +1-858-784-9880. Fax: +1-858-784-9610.

‡ Present address: Max-Delbrück-Center for Molecular Medicine, Robert-Roessle-Str. 10, 13125 Berlin-Buch, Germany.

[1] Abbreviations: Aβ, amyloid β; AFM, atomic force microscopy; Boc-Val-PAM, 4-(*tert*-butoxycarbonyl-valyloxymethyl)-phenylacetic acid; CD, circular dichroism; DIEA, diisopropylethylamine; DIC/HOBt, *N*,*N*′-diisopropylcarbodiimide/*N*-hydroxybenzotriazole; DMAP, 4-dimethylaminopyridine; DMF, dimethylformamide; EOAβ, F19−F20 *E*-olefin mutant of the Aβ 1-40 peptide; NEM, *N*-ethylmaleimide; HBTU, 2-(1*H*-benzotriazole-1-yl)-1,1,3,3-tetramethylaminium hexafluorophosphate; MTT, 3-(4,5-dimethylthiazol-2-yl)-2,5-diphenyltetrazolium bromide; PC12, rat adrenal pheochromocytoma; ThT, thioflavin T, WT, wild type Aβ 1−40 peptide.

10.1021/bi701757v CCC: $40.75
Published on Web 12/14/2007

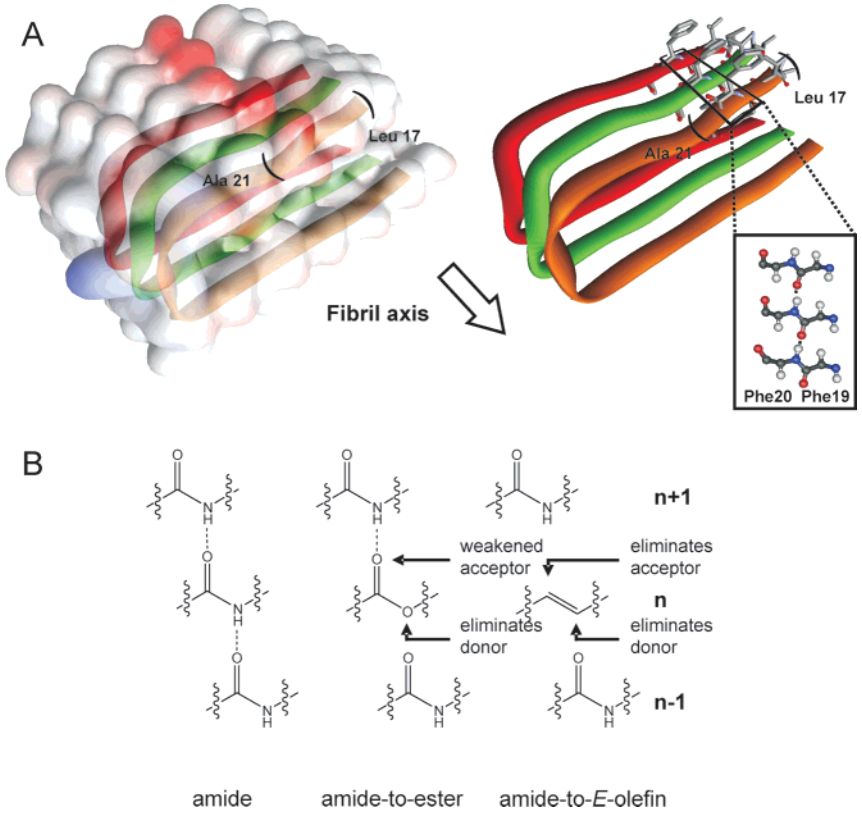

FIGURE 1: (A) Peptide backbone modifications remove intermolecular hydrogen bonds between Aβ 1−40 strands (represented by the differently colored ribbons) within the hydrophobic core region, LVFFA, residues 17−21. Molecular models with and without the depiction of side chain packing are shown (*5*) (Molecular Modeling DataBase accession number: 36199; box: H-bonds formed by the phenylalanines F19−F20). (B) Amide to ester mutations of the peptide backbone eliminate the H-bond donor and weaken the acceptor, while amide-to-*E*-olefin substitutions eliminate both the H-bond donor and acceptor.

quaternary structure formation, as H-bonds in this region become desolvated in the process of amyloid formation. These residues adopt a β-strand conformation and are the most N-terminal residues to be included in one of the two cross β-sheets forming the amyloid core (Figure 1A) (*5*, *7*). Point mutations in this region are highly disruptive to amyloid formation (*12*). Moreover, incorporation of structurally disruptive N-methylated residues in this region result in fibrils with altered morphologies and fibrillization kinetics (*13*). It is thus reasonable to hypothesize that intermolecular hydrogen bonds in this region play a crucial role in stabilizing intermediates on the way to the amyloid fold and especially the structure of amyloid itself, which is a low-energy structure available to numerous peptides and proteins (*14*).

While traditional mutagenesis, enabled by the advent of recombinant DNA technology, has been used heavily by the scientific community to probe the role of side chains in structure acquisition and function, only recently has it become possible to modify the protein backbone in a similar manner to understand the contributions of the amide bonds to folding and assembly energetics, as well as function (*11*, *15*, *16*). The carbonyl and NH comprising the amide bond connecting two amino acid residues in a protein can accept up to two H-bonds and donate one H-bond, respectively (*17*). Protein amide backbone mutagenesis is generally accomplished through the chemical synthesis or semisynthesis of proteins harboring amide-to-ester or amide-to-*E*-olefin substitutions (*11*, *17*).

Energetic comparisons between an all-amide protein and the backbone mutated (ester or *E*-olefin) analogues allow one to study the contribution of specific hydrogen bonds to folding or quaternary structure stability without perturbing the structure of the amino acid side chains, the preferred trans conformation of the amide bond, the configuration of the residue, or the psi−phi dihedral angle preferences in the region of the mutation (*11*, *18*). Amide-to-ester backbone mutations eliminate the amide N−H as a hydrogen bond donor and render the carbonyl a weaker acceptor (Figure 1B) (*18*). Amide-to-*E*-olefin substitutions eliminate both the backbone H-bond acceptor (C═O) and the donor (N−H) (Figure 1B). Amide-to-*E*-olefin and amide-to-ester mutations can be utilized to fairly accurately estimate individual H-bond energies, after correcting the measured perturbation free energies for repulsions between the non-carbonyl oxygen of the ester and the carbonyl oxygen of the amide on the neighboring strand (amide-to-ester mutations) and/or for the desolvation energy differences between an all amide sequence and a sequence containing a single ester or *E*-olefin mutation (*17*, *19*).

We previously communicated that mutating the Phe19−Phe20 backbone amide bond in Aβ 1−40 to an *E*-olefin bond allows the formation of spherical aggregates to the exclusion of amyloid fibrils, suggesting that these two H-bonds in Aβ 1−40 are critical for amyloid fibril formation (*20*). Herein, we further scrutinize the role of H-bonding in amyloidogenesis by carrying out a more extensive amide-to-ester mutagenesis scan through the region of Aβ 1−40 that forms the hydrophobic core within the amyloid fibril, comparing the rates of amyloidogenesis, the seeding competence, and the toxicity of the amide-to-ester variants to wild type Aβ 1−40 and the Phe19−Phe20 *E*-olefin Aβ 1−40 analogue.

MATERIALS AND METHODS

Aβ Peptide Analogue Synthesis. The EOAβ peptide analogue was synthesized as described in (*20*).

Ester analogues L17λ, V18ω, F19ϕ, and F20ϕ of the Aβ 1−40 peptide were prepared using a published Boc/benzyl solid-phase peptide synthesis strategy (α-hydroxy acid incorporation into the sequence is indicated by Greek symbols corresponding to the one-letter code for the analogous α-amino acid) (*21*). Briefly, the synthesis was initiated using 0.1 mmol of Boc-Val-PAM resin (0.8 mmol/g, Advanced Chem Tech), and the chain extension was accomplished using an *in situ* neutralization/HBTU activation procedure, where 5-fold excess of amino acid was preactivated with 4.8 equiv of HBTU and 7 equiv of DIEA in DMF (1.3 mL) for 1.5 min before it was added to the resin. Each coupling step took a minimum of 18 min. The coupling of the α-hydroxy acid to the resin-bound NH_2 was carried out using a DIC/HOBt activation method, where the α-hydroxy acid (0.5 mmol) in 1.3 mL of DCM/DMF (1:1) was activated with DIC (0.5 mmol) in the presence of HOBt (0.6 mmol) at 0 °C for 15 min. The mixture was added to the resin along with NEM (0.2 mmol) and coupled for 15 min at room temperature. The ester bond was formed using a DIC/DMAP activation method where the next amino acid (0.5 mmol) in 1.3 mL of DCM:DMF (1:1) was activated with DIC (0.5 mmol) for 15 min at 0 °C. The mixture was added to the resin followed by NEM (0.2 mmol) and DMAP (2 mg) and coupled for 1 h at room temperature. After the whole synthesis was complete, the peptides were deprotected and cleaved from the resin by treatment with anhydrous HF for 1 h at 0 °C with 5% anisole as a scavenger. The resultant peptide was precipitated with cold diethyl ether, dissolved in acetonitrile:water (1:1), and lyophilized. The crude peptide was purified by HPLC using a 25−50% linear gradient in solvent B over 50 min [Vydac C18 column using solvent A (5% acetonitrile, 95% water, 0.1% TFA) and solvent B (95% acetonitrile, 5% water, 0.1% TFA)]. The purified peptides were analyzed by analytical HPLC, and the masses were verified by MALDI-MS. For ester analogues of Aβ, calculated $(M + H)^+$ 4331, observed: 4331 for analogue L17λ, 4331 for analogue V18ω, 4332 for analogue F19ϕ, 4331 for analogue F20ϕ.

Aβ Peptide Monomerization. The Aβ peptides were pretreated to form monomeric solutions by one of two methods as noted for the particular experiment. For experiments that involved only WT Aβ and/or the EOAβ analogue, a high pH monomerization method was used, as previously described (*22*, *23*). Briefly, WT (purchased from Synpep, Dublin, CA) or EOAβ were dissolved in NaOH at pH 10.5, sonicated, and filtered through both 0.2 μm and 10 kDa cutoff filters (Millipore). Both WT Aβ and the EOAβ analogue gave similar yields of monomeric peptide. For experiments using the ester analogues, which are more sensitive to alkaline hydrolysis, all peptides including WT and EOAβ were pretreated with HFIP. In this HFIP method, kinetic reproducibility of the aggregation time courses was achieved by dissolving the Aβ sequence in HFIP (1 mg/mL), incubating it for 2 h, lyophilizing the HFIP solution, redissolving the resulting solid Aβ in water (1 mg/mL), and subsequently filtering the solution through 0.2 μm and 10 kDa cutoff membrane filters (Millipore). The relative aggregation kinetics of the various Aβ sequences and their ThT fluorescence amplitudes were identical when using either the basic or the HFIP monomerization procedures for both WT and EOAβ peptides; however, utilization of the HFIP protocol reduced the lag phase by ∼30% compared to our previous studies utilizing the high pH procedure (*20*, *22*). Within each experiment, all peptides were pretreated by the same procedure. The figure legends indicate which procedure was used. Peptide concentrations were calculated from absorption measurements at 280 nm using an extinction coefficient of 1280 M^{-1} cm^{-1}.

Thioflavin T Aggregation Assays. Aβ 1−40 peptides were monomerized as described above. For aggregation reactions carried out in a plate reader, peptides (50 μM) were incubated at 37 °C in A-buffer (300 mM NaCl, 50 mM Na-phosphate pH 7.4) with 20 μM ThT added. Thioflavin T fluorescence emission was monitored at 485 nm (excitation at 440 nm) using a fluorescence plate reader (Gemini EM, Molecular Devices). Samples were incubated at 37 °C in low binding 96-well clear bottom plates (Corning), and ThT fluorescence was recorded every 10 min. Samples were agitated for 5 s before each reading. For aggregation reactions under constant agitation, Aβ peptides were incubated in 1.5 mL reaction tubes (50 μM peptide, A-buffer, 37 °C). Agitation was facilitated either by an overhead rotary shaker (20 rpm) or a rocking platform (27 cycles per minute), as indicated in the figure legend. ThT fluorescence was recorded by diluting samples five-fold into A-buffer containing 20 μM ThT and measuring the fluorescence (excitation at 440 nm, emission at 485 nm) with an Aviv ATF-105 Spectrofluorometer (Aviv Biomedical, Lakewood, NJ).

Circular Dichroism. Aβ samples (50 μM) were monomerized by the HFIP method and aggregated either in a plate reader (A-buffer, 37 °C, shaking 5 s every 10 min) or on a rotary shaker (A-buffer, 37 °C, 20 rpm constant agitation) as described in Results. Samples were sonicated for 15 min using a water bath sonicator (FS60, Fisher Scientific). CD spectra of Aβ peptides were recorded at room temperature on an Aviv CD spectrometer as previously described (*22*).

Atomic Force and Electron Microscopy. From an aliquot of the aggregation solution specified in the figure legend, 20 μL was adsorbed to a surface of freshly cleaved mica (5 × 5 mm) for 1 min. The liquid was absorbed into filter paper. Salt and unbound material were removed through three washes by adding 30 μL of water to the mica and immediately absorbing it into filter paper. AFM images were recorded in tapping mode with a Digital Instruments multimode scanning probe microscope with a Nanoscope IIIa controller (Veeco, Woodbury, NY). Likewise, samples for electron microscopy were prepared by adsorbing Aβ samples onto carbon-coated EM grids for 1 min, washing the grid with 3 × 20 μL water, and staining with a 2% uranyl acetate solution for 1 min. EM images were recorded with a Philips CM100 electron microscope operating at an accelerating voltage of 60−80 kV, equipped with a Soft Imaging Systems Keenview CCD camera.

MTT Assay. Aβ peptides were subjected to aggregation on a rotary shaker (monomerized using the HFIP protocol, aggregated at 50 μM peptide concentration, A-buffer, 37 °C, 20 rpm constant agitation) and frozen in acetone/dry ice after the indicated times. Aβ samples were thawed and diluted to final concentrations of 1 μM, 250 nM, and 50 nM in K-12

cell culture media containing 15% horse serum, 5% fetal calf serum, and 1 mM glutamine and were then added to PC12 cell cultures. After 3 d of incubation, metabolic activity was assayed by MTT reduction as previously described (*4*) at three Aβ concentrations; each experiment was performed in triplicate and confirmed in an independent aggregation assay.

RESULTS

To test the hypothesis that hydrogen bonds in the hydrophobic core region of the Aβ amyloid fibril are essential for fibril formation and with the hopes of producing Aβ analogues that can only adopt one or a restricted set of aggregate morphologies, we chemically synthesized four Aβ 1−40 analogues. In these analogues, the amide bonds linking residues 16−20 were replaced one at a time by ester bonds, while retaining the native side chains. This was accomplished experimentally by incorporating the α-hydroxy acid equivalent of the α-amino acid that contributed the N−H to the hydrogen bond of interest into the chain during solid-phase peptide synthesis, which changes the amide bond on the N-terminal side of that residue into an ester-bond. α-Hydroxy acid incorporation into the sequence is denoted by Greek symbols corresponding to the one-letter code for the analogous α-amino acid. Aβ 1−40 L17*λ*, V18*ω*, F19*ϕ*, and F20*ϕ* amide-to-ester analogues were prepared using the Boc/benzyl solid-phase peptide synthesis strategy described in detail previously (*11*). We compared their aggregation time courses, structural characteristics and aggregate morphologies to those of the F19−F20 *E*-olefin mutant of Aβ 1−40 (hereafter referred to as EOAβ) (*20*) and wild type Aβ 1−40 (hereafter referred to as WT).

Aβ 1−40 aggregates into amyloid fibrils by a so-called nucleated polymerization mechanism *in vitro*, in which an energetically unfavorable oligomeric structure, referred to as the nucleus, must form before addition of Aβ monomers becomes thermodynamically favorable (*24*). Since nucleation, associated with a kinetic lag phase, is rate limiting, the presence of small quantities of aggregates larger than the nucleus in the aggregation reaction bypasses the requirement for the nucleation step, thus vastly accelerating or seeding amyloidogenesis. Therefore, it is critical to pretreat Aβ to remove seeds, i.e., to monomerize it quantitatively (see Materials and Methods), so that the aggregation time courses are reproducible. Far-UV circular dichroism (CD) studies of Aβ amide-to-ester mutants monomerized using the HFIP protocol afford spectra consistent with an unstructured ensemble of conformations, a so-called random coil, identical to that of WT monomerized by the HFIP protocol (Figure 2A).

F19ϕ Aβ Aggregation Exhibits a Prolonged Lag Phase, Whereas the Other Amide-to-Ester Variants Aggregate Faster than WT. Amide-to-ester Aβ analogues and WT monomerized by the HFIP procedure were subjected to aggregation assays performed in triplicate at physiological pH (50 μM peptide in A-buffer with 20 μM ThT added, shaking for 5 s every 10 min in a plate reader at 37 °C). Agitation makes Aβ aggregation fast enough to be conveniently observed on a laboratory time scale (*22*). The aggregation of WT and Aβ backbone mutants was monitored by thioflavin T (ThT) fluorescence. ThT is an aromatic

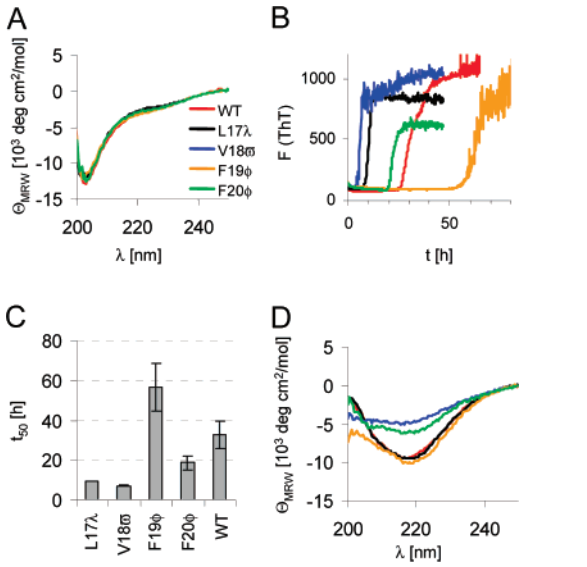

FIGURE 2: (A) Far-UV CD spectra of WT and backbone mutated Aβ peptides at pH 7.4 after the HFIP monomerization pretreatment and prior to aggregation. (B) Aggregation time courses of WT and amide-to-ester backbone Aβ 1−40 mutants monitored by ThT fluorescence. Peptides were monomerized utilizing the HFIP protocol and then incubated at 37 °C (50 μM peptide, A-buffer, 20 μM ThT) while shaking for 5 s every 10 min in a fluorescence plate reader. Aggregation of the F19*ϕ* peptide is delayed compared to the WT. (C) Incubation times (t_{50}) required to reach the half-maximal ThT signal derived from data of the type displayed in panel (B); error bars indicate standard deviations of two sets of triplicate samples. (D) Far-UV CD spectra of the Aβ 1−40 sequences 150 h into the aggregation reaction described in (B).

compound whose fluorescence quantum yield significantly increases upon binding to amyloid and other aggregate structures, including spherical aggregates. The ThT fluorescence curves in Figure 2B represent averages of independent triplicate experiments during the first 80 h of the aggregation time course (aggregation end point = 150 h) (*22*, *25*).

All amide-to-ester Aβ 1−40 variants exhibit time-dependent increases in ThT fluorescence, consistent with aggregation, albeit with variable time courses (Figure 2B). The ThT fluorescence amplitudes achieved are comparable to those exhibited by WT (Figures 2B, S1A, Supporting Information), indicating that similar amounts of amyloid are formed. Aggregation of the L17*λ*, V18*ω*, and F20*ϕ* (the latter has the same amide bond mutated as in EOAβ) Aβ 1−40 amide-to-ester backbone mutants is surprisingly accelerated relative to WT; the amount of time it takes for L17*λ*, V18*ω*, F20*ϕ*, and WT to reach the half-maximal ThT fluorescence amplitude (t_{50}) is 10, 12, 18, and 30 h, respectively, (Figure 2C). In contrast, the F19*ϕ* peptide forms ThT positive aggregates more slowly than WT ($t_{50} \sim 60$ h) under these conditions. Average times for amyloid formation ($t_{50} \pm$ standard deviation) from two experiments each performed in triplicate are presented in Figure 2C. Accelerated amyloidogenesis of L17*λ*, V18*ω*, and F20*ϕ* relative to WT clearly demonstrates that elimination of one hydrogen bond donor from each peptide in the fibril does not preclude the formation of ThT binding competent aggregates. Aggregation of these amide-to-ester Aβ analogues may be accelerated because the free energy penalty is lower for transfer of the amide-to-ester Aβ 1−40 variants from aqueous solution to the core of the amyloid fibril (desolvation) than for the all-amide sequence (*20*). The aggregation kinetics of the amide-

to-ester analogues relative to WT and EOAβ were confirmed independently using a different method of agitation, namely continuous agitation over a time course of 84 h (50 μM peptide in A-buffer, 37 °C, 20 rpm continuous agitation in a rotary shaker following monomerization by the HFIP method). After 1, 4, 18, 22, 30, and 84 h, aliquots were removed and homogenized by sonication in a water bath sonicator (5 min). ThT signals at each time point and far-UV CD spectra (0 h, 18 h, 84 h) were recorded as described in Materials and Methods (Figure S1, Supporting Information).

Amide-to-Ester Aβ Analogues Aggregate into Fibrillar, β-Sheet Rich Structures. Temporal β-sheet structure acquisition of Aβ and its amide-to-ester backbone mutants was monitored by far-UV CD spectroscopy after treatment by the HFIP monomerization protocol. The peptides all exhibit minima in their CD spectra at 207 nm, consistent with unordered structures directly following monomerization (Figure 2A). After 150 h of incubation in a plate reader (50 μM peptide, A-buffer, 37 °C, 5 s of agitation every 10 min), all peptides show CD spectra with minima at 217 nm (Figure 2D), consistent with previously reported spectra of β-sheet rich fibrillar aggregates (*10*, *20*, *26*). The observed differences in CD amplitudes may be due, in part, to light scattering, complicating interpretation. Far UV CD spectra (0 h, 18 h, 84 h) of WT and its amide-to-ester backbone mutant analogues aggregated using continuous agitation in a rotary shaker confirm that all peptides adopt β-sheet rich aggregate structures as aggregation proceeds (Figure S1B−D, Supporting Information). As expected, the appearance of β-sheet secondary structure is delayed in the F19ϕ peptide (Figure S1C, Supporting Information), consistent with the delayed increase in ThT fluorescence (Figure S1A, Supporting Information).

The morphologies of the amide-to-ester Aβ aggregates formed by agitation in a plate reader (50 μM peptide, A-buffer, 37 °C, 5 s of agitation every 10 min) were monitored at the endpoint (150 h) by electron microscopy (EM, Figure 3A). Morphologies of aggregates formed under constant agitation in a rotary shaker (50 μM peptide, A-buffer, 37 °C, 20 rpm of constant agitation) after 18 and 84 h were monitored by atomic force microscopy (AFM, Figures S2, S3, Supporting Information). Morphologies of the final aggregated, β-sheet rich peptides are fibrillar (Figures 3A, S3, Supporting Information), although some differences in fibril length and diameter can be discerned between distinct Aβ peptide backbone mutants. Aβ F19ϕ predominantly forms short, thin straight fibrils early in the aggregation, which later form thickly tangled aggregates, whereas the L17λ peptide forms networks of very long fibrils (>5 μm) early in aggregation (Figure S2, Supporting Information). Western blot analysis of these samples reveals no proteolytic fragments (Figure 3B).

Aβ aggregates formed by agitation for 150 h in a plate reader (50 μM peptide, A-buffer, 37 °C, 5 s of agitation every 10 min) were pelleted by ultracentrifugation at 200 000*g*, and the relative amounts of aggregated and soluble peptides were assessed by SDS-PAGE utilizing Coomassie staining (Figure 3C) and by absorbance at 280 nm (Figure 3D). About 80% of the WT and amide-to-ester variants were found in the pellet fraction, except for the V18ω peptide, where only 50% was in the pellet fraction (Figure 3D). Quantification

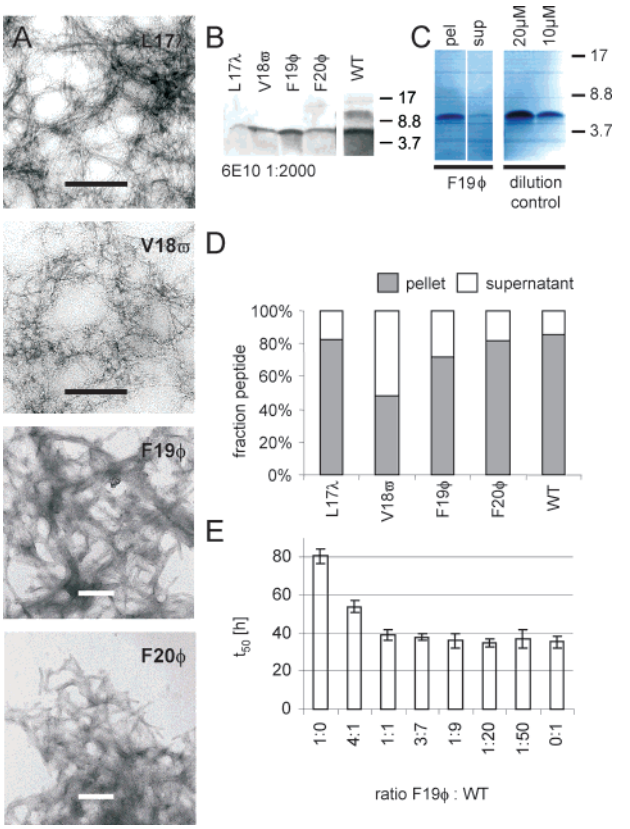

FIGURE 3: (A) Electron microscopy images of amide-to-ester substituted Aβ peptides monomerized by the HFIP method and incubated for 150 h as described in Figure 2B, scale bars 200 nm. (B, C) SDS-PAGE of amide-to-ester mutated Aβ peptides detected by Western blotting (mAb 6E10, B) and Coomassie staining (C) after aggregation under the same conditions. No proteolysis of amide-to-ester mutated peptides was detected. (C) Relative amounts of aggregated and soluble Aβ peptides were determined after a 150 h incubation period by ultracentrifugation (1 h, 200 000*g*) by running supernatants and pellets in a Coomassie stained SDS-PAGE gel (shown: F19ϕ) and comparing the amount of peptide in each sample to a dilution series of WT using densitometry. (D) Relative amounts of the Aβ sequences found in ultracentrifugation supernatants and pellets were determined by absorbance at 280 nm after denaturation with 6 M guanidine hydrochloride. (E) Mixtures of WT and F19ϕ Aβ were subjected to aggregation (50 μM total peptide, A-buffer, 1% DMSO, 20 μM ThT, 37 °C, shaking 5 s every 10 min in a plate reader) and t_{50} values were recorded. F19ϕ does not inhibit the aggregation of WT at substoichiometric concentrations. Error bars indicate standard deviations from a triplicate experiment.

errors were estimated to be ~10%. Also, no peptide fragments were observed on Coomassie stained gels; thus, hydrolysis of the ester bonds does not appear to occur.

F19ϕ Peptide Does Not Inhibit WT Fibril Growth. Since the F19ϕ peptide exhibits a slowed aggregation time course, we tested whether it could slow or inhibit the formation of ThT positive aggregates by WT at substoichiometric concentrations. To test this hypothesis, mixtures of WT and the F19ϕ peptide containing both peptides in ratios from 1:50 to 4:1 (F19ϕ:WT) at a total concentration of 50 μM were aggregated in conditions under which the F19ϕ peptide displayed a t_{50} of 80 h (A-buffer, 20 μM ThT, 1% DMSO, 37 °C, shaking 5 s every 10 min in a plate reader), more than twice that of WT (35 h, Figure 3E). Substoichiometric amounts of F19ϕ do not inhibit aggregation, i.e., the aggregation kinetics of mixtures containing 50% or less F19ϕ

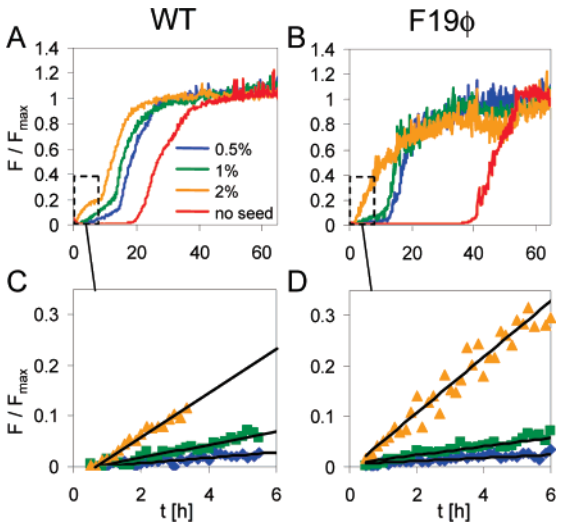

FIGURE 4: Aggregation time courses for seeded reactions monitored by ThT fluorescence. WT (A) and F19ϕ (B) monomerized by the HFIP method were incubated as described in Figure 2B with seeds of WT and F19ϕ fibrils, respectively, added at $t = 0$. Seeds originate from end products of the aggregation of WT (A) or F19ϕ (B) in the time course described in Figure 2B. The end products were sonicated for 30 min and added to the aggregation reaction at final concentrations of 0.5%, 1%, and 2% (w/w). A comparison of the slopes of seeded WT aggregation (C) and seeded F19ϕ aggregation (D) indicate the growth rates are similar for WT and F19ϕ Aβ.

are indistinguishable from WT, whereas t_{50} values of mixtures containing 4:1 F19ϕ:WT lay between those of the two pure peptides. This is consistent with the WT nucleation step being rate-limiting. Once WT seeds form they can recruit WT or F19ϕ to the fibril at nearly equal rates.

To scrutinize this hypothesis, the relative rates of WT and F19ϕ fibril growth were evaluated using a seeded aggregation assay (*22*, *27*), employing fibrillar seeds composed of the same sequence (Figure 4) (50 μM peptide monomerized by the HFIP protocol, A-buffer, 20 μM ThT, 37 °C, shaking 5 s every 10 min in a plate reader). The growth rates of F19ϕ are comparable to WT (Figure 4C,D). Taken together, these findings suggest that the H-bond deletion at F19 inhibits nucleation rather than fibril growth.

Amide-to-E-Olefin Aβ Peptide Analogue Forms Spherical Aggregates. The EOAβ analogue (*20*) and the F20ϕ ester analogue are similar in that they both have a mutated 19−20 amide bond. The F20ϕ backbone mutation eliminates the H-bond donor that makes a hydrogen bond to the neighboring ($n - 1$) Aβ peptide in the fibril (Figure 1B). It should be noted that if the aggregates formed are in-register, then the amide-to-ester mutants will effectively eliminate both the H-bond donor and acceptor functionalities at the location of the mutation. The F20ϕ mutation is not sufficient to inhibit fibril growth or nucleation. The *E*-olefin substitution deletes the 19−20 H-bond donor as well as the H-bond acceptor, so that the intermolecular H-bonds between the preceding ($n - 1$) and the following ($n + 1$) Aβ peptides mediated by the 19−20 amide bond are not possible (Figure 1B). Deletion of the H-bond donor and acceptor in EOAβ is sufficient to preclude nucleation and growth of amyloid fibrils, but not aggregation, as demonstrated below.

As we previously demonstrated, EOAβ self-assembles into spherical aggregates that bind ThT and exhibit fluorescence

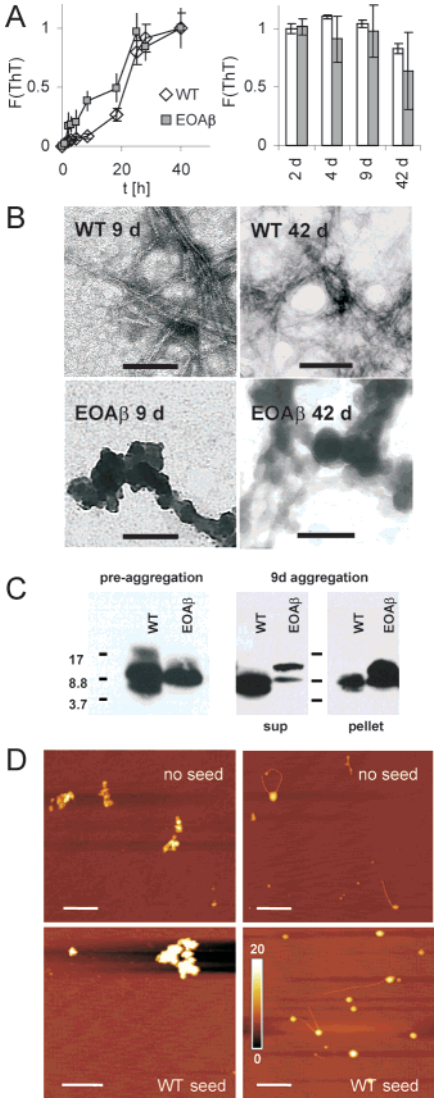

FIGURE 5: Comparison of WT and EOAβ peptide aggregation. (A) These peptides were monomerized using the high pH protocol and were agitated on a rocking platform for 6 weeks (50 μM peptide, A-buffer, 37 °C, 27 cycles per minute, constant agitation). The aggregation kinetics of WT (white diamonds) and EOAβ (gray squares) were monitored by ThT fluorescence. (B) Electron micrographs of samples aggregated for 9 and 42 d show no fibrils in the EOAβ sample; scale bars: 200 nm. (C) WT and EOAβ subjected to 9 d of aggregation were fractionated by ultracentrifugation (1 h, 200 000*g*). SDS-PAGE detected by western blotting (6E10 antibody) of the pellet and the supernatant fractions reveals a degree of aggregation in the EOAβ peptide that is comparable to, if not greater than WT. (D) AFM images of EOAβ (50 μM) representative of the aggregate morphologies observed after 7 d incubation (high pH pretreatment protocol, A-buffer, 37 °C, 20 rpm on rotary shaker) with and without the addition of 3% (w/w) aggregated WT as seeds; scale bar 500 nm, height scale 20 nm. Left panels: spherical aggregates, right panels: small fibers extending from spherical aggregates; spherical aggregates and spherical aggregates sprouting microfibrils were observed in a ratio of ~10:1, respectively.

comparable to that of WT amyloid fibrils (*20*). Aggregation proceeds somewhat faster for the EOAβ than for the WT (Figures 5A, 6A (right panel), and S1A, Supporting Information). However, EOAβ does not populate a fibrillar morphology to an extent that can be detected in EM images ($n = 6$), even after six weeks of continuous agitation (50 μM peptide monomerized by the high pH method, incubated in A-buffer, 37 °C, rocking platform 27 cycles per minute), Figure 5B.

To further scrutinize this finding, EOAβ (50 μM) monomerized by the high pH method was incubated for eight weeks at 37 °C with continuous agitation in a rotary shaker (A-buffer, 0.02% NaN_3, 20 rpm continuous agitation). AFM images were recorded after 7 days ($n = 70$) and after 8 weeks ($n = 48$) to obtain a statistically comprehensive picture of the aggregate morphologies. About 2500 spherical EOAβ aggregates or clumps thereof are present after 7 d, 10% of which sprout thin fibrillar extensions 1.5−2 nm in diameter or display short fibrils (5−6 nm diameter) intimately associated with spherical aggregates (representative images in Figure 5D). Relative amounts and morphologies of aggregates do not increase over the course of 8 weeks (data not shown). In none of the samples do we observe twisted fibrillar aggregates having a diameter of 10−20 nm characteristic of WT fibrils. It is important to note that the distribution of EOAβ aggregate morphologies is not changed by the addition of sonicated WT fibrils (3% w/w) at the beginning of the EOAβ reaction, demonstrating that EOAβ is not competent for fibril growth (Figure 5D), in contrast to the behavior of the amide-to-ester Aβ analogues studied above.

The far UV CD spectra (see ref *20*) of these spherical EOAβ aggregates suggest a β-sheet rich structure, albeit one that differs from the cross β-sheet spectra observed for the fibrillar Aβ aggregates composed of the amide-to-ester Aβ analogues or WT. EOAβ aggregates exhibit a slight shift in their minima toward longer wavelengths (222 vs 218 nm for WT and amide-to-ester Aβ fibrils) and lower amplitude minima. EOAβ and WT peptides monomerized using the high pH method were incubated for 9 d on a rocking platform (50 μM peptide, A-buffer, 37 °C, 27 cycles per minute). The soluble and insoluble fractions were separated by ultracentrifugation (100 000*g*) and were quantified by Western blotting (Figure 5C) and by absorption at 280 nm after denaturing in 6 M guanidine hydrochloride (data not shown). Both methods confirm that an equal, if not greater fraction of the EOAβ sediments at 100 000*g* relative to that of WT. Taken together, these data suggest that the deletion of two crucial H-bonds in the hydrophobic core region prevents the formation of cross β-sheet rich fibrillar structures. However, the backbone mutation in EOAβ stabilizes a ThT-binding spherical aggregate morphology. Interestingly, a spherical aggregate structure is also produced as an intermediate in WT fibrillization and is generated as a metastable structure when WT is treated with cholesterol oxidation products, which promote the aggregation of Aβ peptides by covalent modification of Aβ (*22*, *28*).

EOAβ Spherical Aggregates Can Seed WT Fibrillization; in Contrast, WT Fibrils Cannot Seed EOAβ Fibrillization. The spherical morphology and partial β-sheet structure exhibited by the EOAβ aggregates suggest that their structure may be analogous to the spherical aggregation intermediates formed by WT during its amyloidogenesis. Thus, we wanted to test whether the EOAβ spherical aggregates could hasten WT fibrillization through a seeding mechanism (Figure 6A) (*22*, *29*). As a control, we showed that the addition of WT amyloid fibrils, which had been sonicated for 30 min to form seeds of uniform length, accelerates the rate of WT aggregation (50 μM peptide monomerized using the high pH procedure, A-buffer, 20 μM ThT, 37 °C, shaking 5 s every 10 min in a plate reader) in a concentration-dependent manner (Figure 6B). Notably, addition of EOAβ spherical aggregates accelerates the aggregation of WT under the same reaction conditions (Figure 6C), demonstrating that they suffice to bypass the WT nucleation requirement.

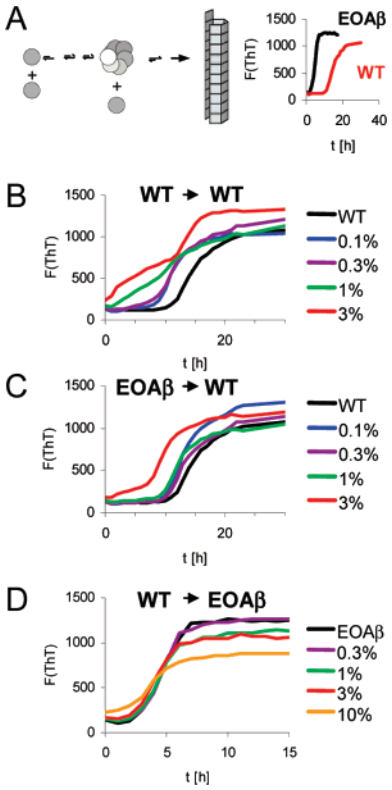

FIGURE 6: EOAβ forms spherical aggregates capable of seeding WT fibrillization, but WT will not seed EOAβ aggregation (fibrillization or spherical aggregate formation). (A) Aβ 1−40 aggregation proceeds by a nucleated polymerization *in vitro*, as described in the introduction. Spherical aggregates could be an intermediate on the pathway to amyloid fibril formation. (A, right) Aggregation kinetics of WT and EOAβ monomerized by the high pH procedure (aggregated with 50 μM peptide, A-buffer, 20 μM ThT, 37 °C, plate reader shaking 5 s every 10 min) were monitored by ThT fluorescence. The aggregation endpoints of the aggregation reactions in A, right were used as seeds in B−D. (B−D) Monomeric WT and monomeric EOAβ were subjected to aggregation as described in (A), with and without the addition of a defined amount of seeds. Seeds formed from WT or EOAβ aggregates (A, right) were sonicated for 30 min prior to addition. (B) WT monomer seeded by WT aggregates and (C) WT monomer seeded by EOAβ aggregates show faster kinetics of aggregation upon addition of seed. (D) In contrast, EOAβ monomer seeded by the addition of WT aggregates does not show an increase in aggregation kinetics.

In striking contrast, WT fibrils that hasten monomeric WT amyloidogenesis do not hasten monomerized EOAβ spherical aggregate formation or seed fibrillization (Figure 6D), even at seed concentrations up to 10% w/w. This result is also in contrast to that observed for spherical aggregates formed by WT in the presence of cholesterol oxidation products, which we have demonstrated to be kinetically competent to efficiently form fibrils from WT seeds (*22*, *28*).

ThT-Positive Aβ Aggregates Exhibit Similar Toxicities Independent of Morphology. An Aβ backbone variant exhibiting delayed fibrillization (F19ϕ) and another that is trapped in a spherical aggregate morphology (EOAβ) are ideally suited to study the cytotoxicity of these Aβ aggregate morphologies in comparison to WT. To probe structure−toxicity relationships, the Aβ 1−40 amide-to-ester mutants,

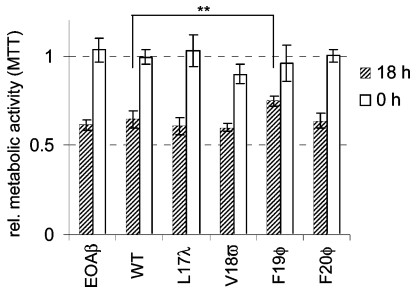

FIGURE 7: WT and Aβ 1−40 backbone mutants, monomerized by the HFIP procedure and subjected to an aggregation reaction (50 μM peptide, A-buffer, 37 °C, 20 rpm constant agitation) as described in Figure S1 (Supporting Information), were added to the culture media of PC12 cells for 3 days (1:300 dilution) after which cellular metabolic capacities were assayed by MTT reduction. F19ϕ significantly ($p < 0.01$) but not substantially reduces metabolic activity compared to WT ($n = 3$). Preaggregation time: white bars $t = 0$ h, striped bars $t = 18$ h.

the EOAβ variant, and WT were monomerized by the HFIP procedure and were aggregated on a rotary shaker (50 μM peptide, A-buffer, 37 °C, 20 rpm, Figure S1, Supporting Information). Aggregates were diluted 1:300 into the medium of rat adrenal pheochromocytoma (PC12) cells. PC12 cells have been used extensively to characterize the toxicity of amyloidogenic peptides and proteins (*4*, *30*). The MTT assay, which monitors the reductive metabolic capacity of the cell (*31*), was used as a surrogate marker for cytotoxicity. To characterize the metabolic capacities at a point in the time course where the extent of aggregation was maximally different, the data in Figure S1A (Supporting Information) were consulted. Samples were removed and frozen at the start as a monomeric control, which should not exhibit toxicity. Samples were removed and frozen after 18 h of incubation, when the differences in ThT signals between F19ϕ, EOAβ, and WT were maximal. Samples were also taken after 84 h of incubation when aggregation was complete for all sequences. The samples were thawed and assayed in the PC12 cells as described above using triplicate samples.

None of the peptides frozen at the beginning of the aggregation induce statistically significant decreases in metabolic activity, as expected of unstructured monomers (Figure 7, white bars). In contrast, all of the peptides reduce the MTT signal in their ThT positive aggregated state 18 h into the time course (Figure 7, striped bars). It is surprising that the toxicities of these sequences, as assessed by metabolic activity, are very similar, despite notable differences in aggregate morphology or extent of aggregation. The *E*-olefin analogue adopts predominantly spherical aggregates at all time points and exhibits cytotoxicity indistinguishable from that of WT fibrils. F19ϕ has only begun to form ThT positive aggregates after 18 h and exhibits a statistically significant ($p < 0.008$) reduced toxicity relative to WT aggregation. However, the differences between F19ϕ and WT cytotoxicity are much smaller than expected. Assaying the impact on cellular metabolic activity of these analogues 84 h into the time course, after completion of aggregation, reveals very similar levels of toxicity for all aggregates (data not shown). These data strongly suggest that either spherical and fibrillar ThT-binding aggregation products have similar toxicities or that there is a common conformation or aggregate morphology that is accessible to all Aβ analogues 18 h into the time course that, in spite of its low overall abundance, is the main mediator of cytotoxicity in this context, measured by metabolic activity.

DISCUSSION

Our study demonstrates that the elimination of one H-bond donor (by amide-to-ester backbone mutagenesis) within the hydrophobic core region of the Aβ amyloid fibril (residues 17−21) is not sufficient to preclude Aβ 1−40 fibrillization, although it does alter the rate of amyloidogenesis, as has also been observed from β-sheet perturbation by the incorporation of non-isostructural N-methylated amino acids at positions 17 and 19 (*13*). In contrast, the one amide-to-*E*-olefin Aβ backbone mutant prepared to date, EOAβ, which eliminates both a H-bond donor and acceptor from each peptide in the hydrophobic core region of the Aβ 1−40 fibril, precludes fibril formation but not aggregation into spherical structures. The *E*-olefin Aβ analogue has the most favorable transfer free energy for fibrillization, much more favorable than the all amide WT sequence and more favorable than the amide-to-ester Aβ variants, which suggests that its loss of H-bonding capacity explains the inability of EOAβ to fibrillize (*19*). Whether eliminating two H-bonds is generally sufficient to block fibrillization will need to be tested by the preparation of additional *E*-olefin Aβ 1−40 variants in the hydrophobic core of the fibril, which, unfortunately, are much more difficult to prepare than the amide-to-ester variants of Aβ studied herein: L17λ, V18ω, F19ϕ, and F20ϕ.

It is very interesting that the EOAβ spherical aggregates can seed WT amyloid fibril formation, whereas WT fibrils cannot seed EOAβ fibrillization, nor can WT fibrils seed EOAβ spherical aggregate formation. While the EOAβ spherical aggregates are competent to nucleate WT fibrillization, it is clear that the EOAβ monomers are not competent to be recruited to a WT seed in a conformation or quaternary structure that promotes fibril growth, presumably because of the loss of two H-bonds in the hydrophobic core. This interpretation is consistent with the fact that fibrils are very rarely observed during EOAβ aggregation, and when they are observed (in 10% of the aggregates), the small fibrillar structures emerging from the spherical aggregates are distinct from WT amyloid fibrils.

The ability of EOAβ spherical aggregates to seed WT fibrillization was not completely unexpected, as we had previously shown that WT spherical aggregates prepared under quiescent conditions with the assistance of oxidative metabolites rapidly form fibrils when shaken, suggesting their kinetic competence for fibrillization and their ability to act as fibril nuclei. Heterologous nucleation has been demonstrated in various amyloidogenic peptides (*32*−*34*).

None of the backbone mutagenized Aβ 1−40 peptides studied herein exhibit toxicity immediately after monomerization using the HFIP protocol as ascertained by a reduced MTT signal, demonstrating that it is unlikely that the unstructured monomers or a defined conformer of the monomer is toxic. In contrast, all of the peptides are toxic, based on a reduced MTT metabolic signal, in their ThT positive aggregated state 18 h into the assembly time course, even though the predominant structures are different: spherical aggregates in the case of EOAβ and incompletely aggregated fibrils in the case of the F19ϕ mutant. Even

though EOAβ cannot adopt a fibrillar aggregate morphology, it exhibits toxicity similar to that of WT, which adopts a predominantly fibrillar morphology under identical conditions. The amide-to-ester Aβ 1−40 variants all adopt at least a partial fibrillar structure 18 h into the aggregation time course and exhibit cytotoxicity that is very similar to WT and EOAβ (Figures 7, S2, Supporting Information).

Considered together, these data strongly suggest that there is a common rare quaternary structure or aggregate morphology that is accessible to all Aβ analogues 18 h into the time course that mediates PC12 cell toxicity. It is also possible, although less likely, that all of the observable aggregate morphologies exhibit similar cytotoxicity. PC12 cell cytotoxicity seems to correlate with other markers of proteotoxicity in AD (primary neuronal survival and long-term potentiation (*35*)); however, structure−cytotoxicity relationships among these Aβ analogues have not been revealed by these other assays.

Our findings are consistent with the emerging idea that it is not the fibrils that exhibit proteotoxicity in Alzheimer's and related protein aggregation diseases. Instead, it appears to be an as yet undefined oligomeric intermediate. This view is corroborated by the appearance of an oligomeric 56 kDa Aβ species that correlates with the appearance of a proteotoxicity phenotype in Alzheimer's disease model mice (*36*), and by the appearance of stable trimeric structures in worm Alzheimer models (ref *4* and unpublished data). Oligomeric Aβ peptide aggregates, which consist of SDS-stable trimers, were also found to inhibit neuronal long-term potentiation (*35*). It is also notable that oligomeric Aβ species of similar morphology and secondary structure as the ones observed for EOAβ are formed in the presence of lipid oxidation products (*23*, *28*). Given that it is now possible to site selectively introduce unnatural amino acids into a given protein in a cell (*16*), backbone mutagenesis technologies could be useful for understanding the structural basis for Aβ cytotoxicity in organismal models of Alzheimer's disease.

ACKNOWLEDGMENT

EM images were taken by D. A. Bosco and I. T. Yonemoto; we thank M. R. Ghadiri for use of his AFM.

SUPPORTING INFORMATION AVAILABLE

Aggregation of Aβ and its backbone variant analogues mediated by agitation on a rotary shaker (50 μM peptide monomerized by the HFIP protocol and aggregated in A-buffer, 37 °C, 20 rpm constant agitation, monitored by ThT fluorescence) for use in toxicity assays and CD (Figure S1). AFM images of WT, EOAβ, and the amide-to-ester Aβ 1−40 analogues aggregated as described in Figure S1 for 18 h (Figure S2) and 84 h (Figure S3) are shown. This material is available free of charge via the Internet at http://pubs.acs.org.

REFERENCES

1. Tanzi, R. E., and Bertram, L. (2005) Twenty years of the Alzheimer's disease amyloid hypothesis: a genetic perspective, *Cell 120*, 545−555.
2. Haass, C., and Selkoe, D. J. (2007) Soluble protein oligomers in neurodegeneration: lessons from the Alzheimer's amyloid beta-peptide, *Nat. Rev. Mol. Cell Biol. 8*, 101−112.
3. Lashuel, H. A., Hartley, D., Petre, B. M., Walz, T., and Lansbury, P. T., Jr. (2002) Neurodegenerative disease: amyloid pores from pathogenic mutations, *Nature 418*, 291.
4. Cohen, E., Bieschke, J., Perciavalle, R. M., Kelly, J. W., and Dillin, A. (2006) Opposing activities protect against age-onset proteotoxicity, *Science 313*, 1604−1610.
5. Luhrs, T., Ritter, C., Adrian, M., Riek-Loher, D., Bohrmann, B., Dobeli, H., Schubert, D., and Riek, R. (2005) 3D structure of Alzheimer's amyloid-beta(1−42) fibrils, *Proc. Natl. Acad. Sci. U.S.A. 102*, 17342−17347.
6. Tycko, R. (2006) Molecular structure of amyloid fibrils: insights from solid-state NMR, *Q. Rev. Biophys. 39*, 1−55.
7. Petkova, A. T., Buntkowsky, G., Dyda, F., Leapman, R. D., Yau, W. M., and Tycko, R. (2004) Solid state NMR reveals a pH-dependent antiparallel beta-sheet registry in fibrils formed by a beta-amyloid peptide, *J. Mol. Biol. 335*, 247−260.
8. Blake, C., and Serpell, L. (1996) Synchrotron X-ray studies suggest that the core of the transthyretin amyloid fibril is a continuous beta-sheet helix, *Structure 4*, 989−998.
9. Nelson, R., and Eisenberg, D. (2006) Recent atomic models of amyloid fibril structure, *Curr. Opin. Struct. Biol. 16*, 260−265.
10. Fowler, D. M., Koulov, A. V., Alory-Jost, C., Marks, M. S., Balch, W. E., and Kelly, J. W. (2006) Functional amyloid formation within mammalian tissue, *PLoS Biol. 4*, e6.
11. Deechongkit, S., Nguyen, H., Powers, E. T., Dawson, P. E., Gruebele, M., and Kelly, J. W. (2004) Context-dependent contributions of backbone hydrogen bonding to beta-sheet folding energetics, *Nature 430*, 101−105.
12. Esler, W. P., Stimson, E. R., Ghilardi, J. R., Lu, Y. A., Felix, A. M., Vinters, H. V., Mantyh, P. W., Lee, J. P., and Maggio, J. E. (1996) Point substitution in the central hydrophobic cluster of a human beta-amyloid congener disrupts peptide folding and abolishes plaque competence, *Biochemistry 35*, 13914−13921.
13. Sciarretta, K. L., Boire, A., Gordon, D. J., and Meredith, S. C. (2006) Spatial separation of beta-sheet domains of beta-amyloid: disruption of each beta-sheet by N-methyl amino acids, *Biochemistry 45*, 9485−9495.
14. Fandrich, M., Fletcher, M. A., and Dobson, C. M. (2001) Amyloid fibrils from muscle myoglobin, *Nature 410*, 165−166.
15. Dawson, P. E., Muir, T. W., Clark-Lewis, I., and Kent, S. B. (1994) Synthesis of proteins by native chemical ligation, *Science 266*, 776−779.
16. Liu, W., Brock, A., Chen, S., and Schultz, P. G. (2007) Genetic incorporation of unnatural amino acids into proteins in mammalian cells, *Nat. Methods 4*, 239−244.
17. Powers, E. T., Deechongkit, S., and Kelly, J. W. (2005) Backbone-Backbone H-Bonds Make Context-Dependent Contributions to Protein Folding Kinetics and Thermodynamics: Lessons from Amide-to-Ester Mutations, *Adv. Protein Chem. 72*, 39−78.
18. Koh, J. T., Cornish, V. W., and Schultz, P. G. (1997) An experimental approach to evaluating the role of backbone interactions in proteins using unnatural amino acid mutagenesis, *Biochemistry 36*, 11314−11322.
19. Fu, Y., Gao, J., Bieschke, J., Dendle, M. A., and Kelly, J. W. (2006) Amide-to-*E*-olefin versus amide-to-ester backbone H-bond perturbations: Evaluating the O−O repulsion for extracting H-bond energies, *J. Am. Chem. Soc. 128*, 15948−15949.
20. Fu, Y., Bieschke, J., and Kelly, J. W. (2005) *E*-olefin dipeptide isostere incorporation into a polypeptide backbone enables hydrogen bond perturbation: probing the requirements for Alzheimer's amyloidogenesis, *J. Am. Chem. Soc. 127*, 15366−15367.
21. Beligere, G. S., and Dawson, P. E. (2000) Design, Synthesis, and Characterization of 4-Ester CI2, a Model for Backbone Hydrogen Bonding in Protein α-Helices, *J. Am. Chem. Soc. 122*, 12079−12082.
22. Bieschke, J., Zhang, Q., Powers, E. T., Lerner, R. A., and Kelly, J. W. (2005) Oxidative metabolites accelerate Alzheimer's amyloidogenesis by a two-step mechanism, eliminating the requirement for nucleation, *Biochemistry 44*, 4977−4983.
23. Siegel, S. J., Bieschke, J., Powers, E. T., and Kelly, J. W. (2007) The oxidative stress metabolite 4-hydroxynonenal promotes

Alzheimer protofibril formation, *Biochemistry 46*, 1503−1510.
24. Jarrett, J. T., and Lansbury, P. T., Jr. (1993) Seeding "one-dimensional crystallization" of amyloid: a pathogenic mechanism in Alzheimer's disease and scrapie? *Cell 73*, 1055−1058.
25. Levine, H., 3rd. (1995) Soluble multimeric Alzheimer beta(1−40) pre-amyloid complexes in dilute solution, *Neurobiol. Aging 16*, 755−764.
26. Post, K., Pitschke, M., Schafer, O., Wille, H., Appel, T. R., Kirsch, D., Mehlhorn, I., Serban, H., Prusiner, S. B., and Riesner, D. (1998) Rapid acquisition of beta-sheet structure in the prion protein prior to multimer formation, *Biol. Chem. 379*, 1307−1317.
27. Collins, S. R., Douglass, A., Vale, R. D., and Weissman, J. S. (2004) Mechanism of prion propagation: amyloid growth occurs by monomer addition, *PLoS Biol. 2*, e321.
28. Zhang, Q., Powers, E. T., Nieva, J., Huff, M. E., Dendle, M. A., Bieschke, J., Glabe, C. G., Eschenmoser, A., Wentworth, P., Jr., Lerner, R. A., and Kelly, J. W. (2004) Metabolite-initiated protein misfolding may trigger Alzheimer's disease, *Proc. Natl. Acad. Sci. U.S.A. 101*, 4752−4757.
29. Catalano, S. M., Dodson, E. C., Henze, D. A., Joyce, J. G., Krafft, G. A., and Kinney, G. G. (2006) The role of amyloid-beta derived diffusible ligands (ADDLs) in Alzheimer's disease, *Curr. Top. Med. Chem. 6*, 597−608.
30. Bucciantini, M., Giannoni, E., Chiti, F., Baroni, F., Formigli, L., Zurdo, J., Taddei, N., Ramponi, G., Dobson, C. M., and Stefani, M. (2002) Inherent toxicity of aggregates implies a common mechanism for protein misfolding diseases, *Nature 416*, 507−511.
31. O'Brien, J., Wilson, I., Orton, T., and Pognan, F. (2000) Investigation of the Alamar Blue (resazurin) fluorescent dye for the assessment of mammalian cell cytotoxicity, *Eur. J. Biochem. 267*, 5421−5426.
32. Peim, A., Hortschansky, P., Christopeit, T., Schroeckh, V., Richter, W., and Fandrich, M. (2006) Mutagenic exploration of the cross-seeding and fibrillation propensity of Alzheimer's beta-amyloid peptide variants, *Protein Sci. 15*, 1801−1805.
33. Lundmark, K., Westermark, G. T., Olsen, A., and Westermark, P. (2005) Protein fibrils in nature can enhance amyloid protein A amyloidosis in mice: Cross-seeding as a disease mechanism, *Proc. Natl. Acad. Sci. U.S.A. 102*, 6098−6102.
34. Derkatch, I. L., Uptain, S. M., Outeiro, T. F., Krishnan, R., Lindquist, S. L., and Liebman, S. W. (2004) Effects of Q/N-rich, polyQ, and non-polyQ amyloids on the de novo formation of the [PSI+] prion in yeast and aggregation of Sup35 in vitro, *Proc. Natl. Acad. Sci. U.S.A. 101*, 12934−12939.
35. Walsh, D. M., Klyubin, I., Fadeeva, J. V., Cullen, W. K., Anwyl, R., Wolfe, M. S., Rowan, M. J., and Selkoe, D. J. (2002) Naturally secreted oligomers of amyloid beta protein potently inhibit hippocampal long-term potentiation in vivo, *Nature 416*, 535−539.
36. Lesne, S., Koh, M. T., Kotilinek, L., Kayed, R., Glabe, C. G., Yang, A., Gallagher, M., and Ashe, K. H. (2006) A specific amyloid-beta protein assembly in the brain impairs memory, *Nature 440*, 352−357.

BI701757V